Int. J. Heat Mass Transfer. Vol. 30, No. 9, pp. 1787–1801, 1987
Printed in Great Britain

0017–9310/87 $3.00 + 0.00

Numerical prediction of turbulent plane jets and forced plumes by use of the k–ε model of turbulence

J. F. SINI and I. DEKEYSER

Institut de Mécanique Statistique de la Turbulence, Université d'Aix-Marseille II, Unité Mixte Université–CNRS No. 380033, 12 Avenue du Général Leclerc, 13003 Marseille, France

(*Received for publication* 5 *December* 1986)

Abstract—A buoyancy-extended k–ε model of turbulence has been developed for calculating the dynamical and thermal fields in plane turbulent jets and forced plumes in a uniform stagnant environment. The governing partial differential equations (continuity, lateral and longitudinal momentum, thermal energy, turbulent kinetic energy k and its dissipation rate ε) are solved by means of an efficient computer program (called JEPHTE) for elliptic unsteady differential equations. A version assuming C_μ to be an empirical function of the densimetric Froude number at the source has been tested. The predictions are compared with experimental data and/or computed results obtained with more complex modellings of the buoyancy effects.

1. INTRODUCTION

THE PROBLEM of reducing the pollution in the atmosphere and water is a serious concern for scientists and engineers. In order to minimize the impact of some unavoidable emission of pollutants into our environment, the dispersion of pollutants should be predictable. The fluid motion governing this dispersion is mostly turbulent and under gravitational influence, and so, it is important to study turbulent buoyant flows and develop reliable methods for their prediction.

This paper is concerned with the calculation of turbulent jets and forced plumes issuing vertically into uniform stagnant surroundings. The flows considered are two-dimensional and the buoyant jet is generated by discharging lighter fluid vertically upwards. To close the mean-flow equations a k–ε turbulence model has been introduced so as to determine the unknown terms representing the turbulent fluxes of heat and momentum. The k–ε model involves the solution of transport equations for the turbulence energy k and its dissipation rate ε.

One way of accounting for buoyancy in this model makes use of the algebraic-stress model (ASM) approach [1]. It has been tested successfully by many workers [2, 3]. Modelled transport equations for the Reynolds stresses and heat fluxes are simplified to yield algebraic relations. The buoyancy terms also appear in these relations, leading effectively to non-isotropic eddy viscosities and diffusivities as functions of some local Froude number. This modelling automatically results in a buoyancy influence on C_μ [2].

In the present work, the buoyancy effects are accounted for by including buoyancy terms in the k and ε equations without using the ASM approach. This 'standard' k–ε model has been widely tested and is capable of predicting a fairly large variety of hydraulic flow situations with the same empirical input. Complete universality of the empirical set of constants cannot and should not be expected, and experience has shown that even in certain fairly simple flows some of them require different values.

Using the constant value $C_\mu = 0.09$, this paper shows (Section 4.1) that the development of thermal and dynamical mean fields is correctly predicted in a plane non-buoyant jet, where temperature may be considered as a passive contaminant. On the other hand, in the case of a pure plume, flow completely dominated by the buoyancy forces, the centre-line velocity is over-estimated by about 20%. Because non-buoyant jet and pure plume are the two limiting forms of the heated jet, the k–ε model has been extended so that all plane jets can be predicted with the same empirical input. Thus a version assuming C_μ to be an empirical function of the discharge Froude number has been tested.

This paper deals with the application of the buoyancy-extended k–ε model to the calculation of turbulent plane jets and forced plumes in uniform stagnant surroundings and comparisons are made between prediction and experiment. Section 2 provides a presentation of the physical and mathematical model and Section 3 presents a statement of the boundary conditions together with a brief description of the solution method. Comparison between model simulations and experimental data is provided in Section 4, while concluding remarks are presented in Section 5.

NOMENCLATURE

$A_W, A_\theta, A_k, A_\varepsilon$ axial decay constants for velocity (equation (24)), temperature (equation (25)), turbulent kinetic energy (equation (26)), dissipation rate (equation (27)) in a pure jet

$B_W, B_\theta, B_k, B_\varepsilon$ axial decay constants for velocity (equation (30)), temperature (equation (31)), turbulent kinetic energy (equation (32)), dissipation rate (equation (33)) in a pure plume

B buoyancy production/destruction of k (equation (13))

C term of convection in k-equation (equation (11)), $U_j(\partial k/\partial x_j)$

C_μ constant in the turbulence model (equation (10))

$C_{\varepsilon 1}, C_{\varepsilon 2}$ constants in the turbulence model (equation (17))

D term of diffusion in k-equation (equation (14))

D_0 jet/plume exit width (Fig. 3)

F discharge densimetric Froude number (equation (21))

G jet/plume exit Grashof number (equation (20))

g_j components of gravitational acceleration $(0, 0, -g)$

g gravitational acceleration

H_0 height of the vertical slot's wall (Fig. 1)

K_T turbulent (or eddy) diffusivity (equation (6))

k turbulent kinetic energy per unit mass (equation (11))

P mean pressure (equation (2))

$\mathscr{P}$ stress production of k (equation (12))

Pr_T turbulent Prandtl number (equation (7))

p fluctuating pressure (equation (14))

Re jet-plume exit Reynolds number (equation (19))

S_{W_j}, S_{W_p} spreading parameters for velocity field in pure jet (equation (22)), pure plume (equation (28))

$S_{\theta_j}, S_{\theta_p}$ spreading parameters for temperature field in pure jet (equation (23)), pure plume (equation (29))

t time

U_j components of mean velocity in tensor notation

U horizontal mean velocity

u_j components of fluctuating velocity in tensor notation

$\overline{u_i u_j}$ turbulent shear stresses in tensor notation

$\overline{u_j\theta}$ turbulent heat flux in x_j-direction

$\mathscr{W}$ time-mean square of the vorticity fluctuation [20]

W vertical mean velocity

W_r velocity scale (equation (34))

$\overline{w\theta}$ vertical turbulent heat flux

x_j Cartesian coordinates in tensor notation (Fig. 1)

x cross-stream (horizontal) coordinate

x_s location of vertical symmetry line (Fig. 3)

z longitudinal (vertical) coordinate

z_0 location of virtual origin (Fig. 3)

z_r length scale (equation (34)).

Greek symbols

β volumetric expansion coefficient, (equation (4)), $(1/\rho)(\partial\rho/\partial\Theta)_\rho$

$\Delta\Theta$ mean temperature excess, $\Theta - \Theta_N$

$\Delta\Theta_r$ temperature scale (equation (34))

δ_{ij} Krönecker delta: 1 for $i = j$; 0 for $i \neq j$

δ velocity half-width, i.e. values of x at which $W = W_m/2$ (Fig. 3)

δ_θ temperature half-width, i.e. values of x at which $\Delta\Theta = \Delta\Theta_m/2$ (Fig. 3)

ε rate of dissipation of k (equation (17))

η similarity coordinate, $(x - x_s)/\delta$

η_θ similarity coordinate, $(x - x_s)/\delta_\theta$

ν molecular kinematic viscosity (equation (19))

ν_T turbulent (or eddy) viscosity (equation (5))

ρ fluid density (equation (4))

σ_k constant in the turbulence model (equation (16))

σ_ε constant in the turbulence model (equation (17))

Θ mean temperature (equation (3))

$\overline{\theta^2}$ mean square temperature fluctuation.

Subscripts

$\mathfrak{C}$ centre-line value

i, j indices in tensor notation or finite-difference integers (Fig. 2)

m maximum value

N natural (initial) ambient value

0 value at the jet/plume exit

r reference value (equation (34)).

2. THE PHYSICAL AND MATHEMATICAL MODEL

The fluid is assumed to be incompressible. The difference between the time-averaged local fluid density ρ and the ambient density ρ_N is small, so that $|\rho-\rho_N|/\rho_N \ll 1$ in buoyant jets. Thus using the ambient density ρ_N instead of the local density ρ produces a small error in the description of the inertial force. However, the difference $|\rho-\rho_N|$ may be important in the description of the gravitational body forces.

This so-called Boussinesq assumption will be adopted in the rest of this paper. This means that attention is restricted to cases in which the induced density deviations are small compared to the total fluid density; it is so for most environmental applications.

Under these assumptions, the time-averaged equations governing the velocity and temperature distribution in two-dimensional plane vertical buoyant jets or plumes may be written as

$$\frac{\partial U_j}{\partial x_j} = 0 \tag{1}$$

$$\frac{\partial U_i}{\partial t} + U_j\frac{\partial U_i}{\partial x_j} = \frac{\rho-\rho_N}{\rho_N}g_i - \frac{1}{\rho_N}\frac{\partial P}{\partial x_i} - \frac{\partial \overline{u_iu_j}}{\partial x_j} \tag{2}$$

$$\frac{\partial \Theta}{\partial t} + U_j\frac{\partial \Theta}{\partial x_j} = -\frac{\partial \overline{u_j\theta}}{\partial x_j} \tag{3}$$

where equation (1) is the continuity equation, equations (2) the momentum equations and equation (3) the temperature equation. As is usual for these kinds of fully turbulent flows the molecular transport terms have been neglected since they are small when compared with those of turbulent transport.

The present version of the model does not include a conservation equation for some species concentration and therefore the density difference term in equation (2) is only related to the temperature of the fluid through the following linear equation of state:

$$\frac{\rho-\rho_N}{\rho_N} = -\beta(\Theta-\Theta_N) \tag{4}$$

where β is the thermal expansion coefficient of the fluid. β may be a function of Θ, but is assumed constant to a good approximation for cases with limited temperature ranges (for other cases see ref. [4]).

The numerical solution of the above set of equations requires the introduction of additional expressions or additional transport equations for the turbulent shear stresses $\overline{u_iu_j}$ and the turbulent heat fluxes $\overline{u_j\theta}$. For the k–ε model adopted in the present work, $\overline{u_iu_j}$ and $\overline{u_j\theta}$ are computed using the eddy viscosity and eddy diffusivity concepts, thus

$$-\overline{u_iu_j} = \nu_T\left(\frac{\partial U_i}{\partial x_j} + \frac{\partial U_j}{\partial x_i}\right) - \frac{2}{3}\delta_{ij}k \tag{5}$$

and

$$-\overline{u_j\theta} = K_T\frac{\partial \Theta}{\partial x_j} \tag{6}$$

where ν_T is the eddy viscosity and K_T the eddy diffusivity.

Experiments indicate that ν_T and K_T are not constants but vary in a flow and from one flow to another, but their ratio

$$Pr_T = \frac{\nu_T}{K_T} \tag{7}$$

which is the turbulent Prandtl number, is approximately constant. In the present work Pr_T is assumed to be constant and the value adopted is defined below. So the closure problem is now shifted to determining the distribution of ν_T.

The k–ε model characterizes the local state of turbulence by the turbulent kinetic energy k and its rate of dissipation ε. The eddy viscosity coefficient ν_T is evaluated using the Prandtl–Kolmogorov hypothesis

$$\nu_T \propto Lk^{1/2} \tag{8}$$

where L is the turbulence length scale or mixing length. Moreover, the energy dissipation ε is modelled by the Kolmogorov relation

$$\varepsilon \propto \frac{k^{3/2}}{L}. \tag{9}$$

We shall adopt the commonly made assumption that the length scales in expressions (8) and (9) are equal [1], yielding the basic relation

$$\nu_T = C_\mu\frac{k^2}{\varepsilon} \tag{10}$$

where C_μ must be empirically fixed.

The turbulent kinetic energy k is obtained from the following transport equation:

$$\frac{\partial k}{\partial t} + U_j\frac{\partial k}{\partial x_j} = \mathscr{P} + B + D - \varepsilon \tag{11}$$

where $\mathscr{P}$ is the rate of shear production of turbulence energy

$$\mathscr{P} = -\overline{u_iu_j}\frac{\partial U_i}{\partial x_j} \tag{12}$$

B the rate of buoyancy production/destruction of turbulence energy

$$B = -\beta g_j\overline{u_j\theta} \tag{13}$$

ε the dissipation rate of k, and D the direct dissipation by diffusive transport

$$D = -\frac{\partial}{\partial x_j}\left[\overline{\frac{u_mu_m}{2}u_j} - \nu\frac{\partial k}{\partial x_j} + \overline{\frac{pu_i}{\rho_N}}\delta_{ij}\right]. \tag{14}$$

At high turbulent Reynolds numbers molecular diffusion is negligible so that the diffusive transport of kinetic energy, equation (14), is reduced to

Table 1. Values of the constants in the k–ε model

$C_\mu(\infty)$	σ_k	σ_ε	C_{ε_1}	C_{ε_2}
0.09	1.0	1.3	1.44	1.92

$$D = -\frac{\partial}{\partial x_j}\left[\frac{\overline{u_m u_m}}{2}u_j + \frac{\overline{pu_i}}{\rho_N}\delta_{ij}\right]. \quad (15)$$

The model, which is in common use [8], consists of a simple gradient type representation

$$\frac{\overline{u_m u_m}}{2}u_j + \frac{\overline{pu_i}}{\rho_N} = -\frac{\nu_T}{\sigma_k}\frac{\partial k}{\partial x_j} \quad (16)$$

where σ_k is an empirical constant to be defined later.

The closure of the model for calculating the dynamical field is completed through the following equation for the turbulence energy dissipation rate [9]:

$$\frac{\partial \varepsilon}{\partial t} + U_j\frac{\partial \varepsilon}{\partial x_j} = C_{\varepsilon_1}\frac{\varepsilon}{k}(\mathscr{P}+B) - C_{\varepsilon_2}\frac{\varepsilon^2}{k} + \frac{\partial}{\partial x_j}\left(\frac{\nu_T}{\sigma_\varepsilon}\frac{\partial \varepsilon}{\partial x_j}\right). \quad (17)$$

The value of the constant C_μ appearing in equation (10) was chosen with reference to non-buoyant local-equilibrium shear layers where the production $\mathscr{P}$ and the dissipation ε are in approximate balance. For these flow equations, equations (5), (10) and (12) can be combined to $C_\mu = (\overline{u_1 u_2}/k)^2$ and measurements yielded $\overline{u_1 u_2}/k \simeq 0.3$ so that $C_\mu = 0.09$.

In fact, universality of the constant C_μ cannot and should not be expected: it may acquire a somewhat different value even in certain fairly simple flows [5].

As will be seen in Section 4.2, the numerical results concerning the centre-line velocity decay of the vertical pure plume is overpredicted by about 20% when using the standard value $C_\mu = 0.09$.

The following functional relationship has been introduced in order to make C_μ sensitive to the buoyancy discharge

$$C_\mu(F) = 0.09 + 0.04[1 + \tanh(2\log F^{-1} + 3)] \quad (18)$$

so that $C_\mu(\infty) = 0.09$ if the discharge Froude number F tends to infinity (pure jet) and increases to 0.17 when $F = 0$ (pure plume). Relation (18), devised on an entirely empirical basis without physical interpretation or justification, significantly improves the k–ε model's ability to predict plane buoyant jets issuing in uniform stagnant surroundings [6].

The constant value of the turbulent Prandtl number Pr_T, namely 0.4, has been determined by comparing predictions with experimental data of the centre-line mean thermal intensity decay in a heated vertical jet [7]. This optimized value is to be compared with the 0.5 recommended by Chen and Rodi [3] in their review of experimental data for vertical buoyant jets.

The values of the five empirical constants in the k–ε model are listed in Table 1. The values of the constants σ_k and σ_ε were taken from Launder and Spalding [10, 11]. The values retained for the coefficients C_{ε_1} and C_{ε_2} are those recommended by Rodi [1].

3. SOLUTION OF EQUATIONS

The previous section has outlined a closed system of elliptic partial differential equations which can of course be solved for the present problem only when the relevant initial and boundary conditions have been specified.

3.1. *Boundary and initial conditions*

For all the cases considered in the present work, plane jet or plume vertically discharged into initially stagnant surroundings, the flow is symmetrical to the jet (or plume) axis and so calculations can be performed only over half of the flow. The definition sketch of the rectangular calculation domain is shown in Fig. 1.

The right-hand boundary of the solution domain coincides with the symmetry line $x = x_s$. On this boundary all variables, except the U velocity which is equal to zero, have a zero x-gradient.

At the left-hand boundary ($x = 0$) and the upper boundary ($z = z_{max}$), Neumann conditions are imposed for U, W, Θ, k and ε. At the lower boundary ($z = 0$) and the vertical nozzle's wall ($x = x_s - D_0/2$, $0 < z < H_0$), zero values are prescribed for U, W, k and ε whereas the temperature is set equal to the constant ambient value.

At the source of the jet (or plume) located at $z = H_0$ and $x_s - D_0/2 < x < x_s$ the distribution of all dependent variables must be specified. Unfortunately, measured exit profiles for velocity W_0 and temperature Θ_0 were not available so that uniform profiles have been assumed. The shapes and levels of k and ε exit profiles are those chosen by Sini [6] so as to obtain the best numerical prediction of a non-buoyant plane jet with a second-order moment closure model. Near the edge of the nozzle, the presence of the wall boundary induces rather sharp turbulence intensity profiles, the levels of k and ε were chosen as $k_{m_0}/W_0^2 = 2.0 \times 10^{-2}$ and $\varepsilon_{m_0} D_0/W_0^3 = 1.6 \times 10^{-3}$. Out of this boundary region, the turbulence exit profiles are assumed to be flat with relatively low levels namely $k_0 = 0.14 k_{m_0}$ and $\varepsilon_0 = 0.02\varepsilon_{m_0}$.

Initially, the ambient fluid is assumed to be of uniform density and motionless with weak homogeneous turbulence intensities; k_0 and ε_0 are assigned all over the calculation domain.

3.2. *Solution procedure*

A finite difference approximation has been used. The finite difference mesh is regular and each rectangular cell of dimension $\Delta x\,\Delta z$ is located by the position of its centre: $(i-3/2)\Delta x$, $(j-3/2)\Delta z$. The boundary conditions are specified in the dashed fictive cells which border the calculation domain (Fig. 2). The spatial discretization makes use of a staggered grid (Fig. 2): the velocity components are defined for the centres of the cell sides while all other scalar dependent variables are defined at the centre point of the cell.

The computer program, code-named JEPHTE,

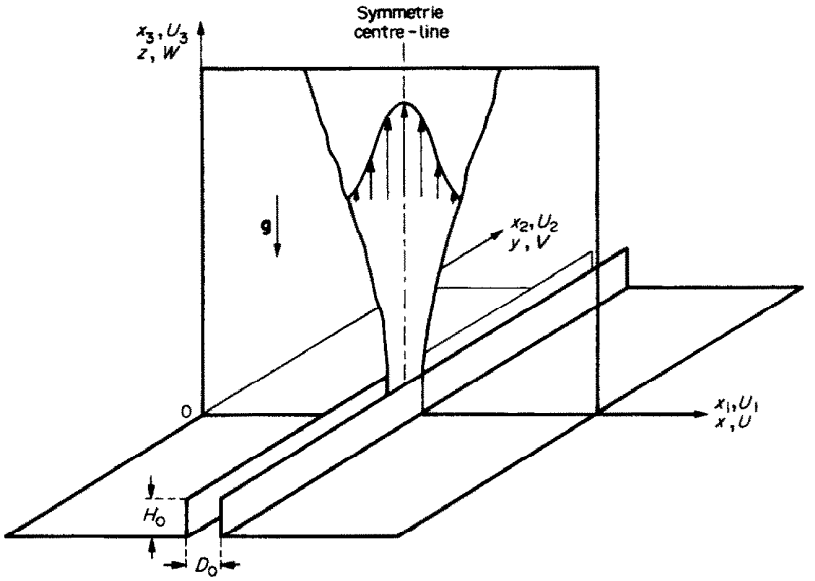

FIG. 1. Definition sketch of the calculation domain.

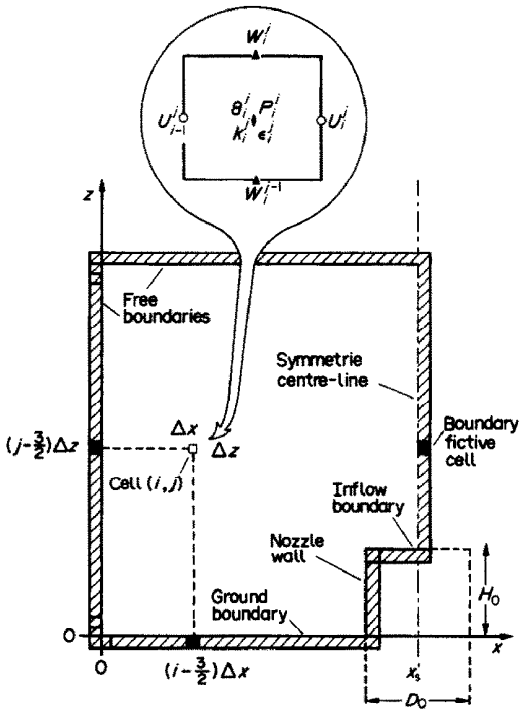

FIG. 2. Boundaries of the calculation domain (the boundary conditions are specified in external dashed fictive cells). The upper sketch shows the staggered grid and the location of the nodes where dependent variables are defined.

developed at I.M.S.T. uses the M.A.C. method [12] as presented by Hirt and Harlow [13]. The numerical procedure, explicit in time, uses centred differences for the diffusion terms and an upwind-weighted scheme for the advection terms. At each time step, the divergence condition (continuity) on mean velocities is directly satisfied by the mean of the artificial compressibility method described by Chorin [14]. This implicit iterative method lies in simultaneous relaxing velocity and pressure fields and is equivalent to solving a Poisson equation for the pressure [15]. Since the numerical methods involved are now well known they will not be developed further here, for further details see for example Gaillard [16] or Sini [6].

The time-dependent problem was run from the initial state to a final steady state by continuing the process till quantities ceased to change with time. This paper deals only with numerical results obtained in the steady state for which experimental data are available.

With a grid size of 5000 nodes, a typical calculation took approximately 2000 time steps to obtain the steady-state solution, requiring about 220K-words of core store and an execution time of 2 min on a CRAY-1 S-1000 computer.

4. PRESENTATION AND DISCUSSION OF RESULTS

In the previous sections a mathematical model was described which will now be used to simulate turbulent forced plumes (or buoyant jets) generated from a linear source which emits a flux of buoyancy and momentum, exhausting into uniform and stagnant surroundings. The buoyancy force acts in the direction of the jet velocity at the source.

The flow is governed by the relative importance of the buoyancy and the momentum fluxes at the source. When buoyancy effects are negligible, the jet is governed by the momentum flux only and is called 'pure jet' or simply 'jet'. The other limiting case, in which the buoyancy effects completely dominate the flow, is termed 'pure plume'. These two limiting flow situations are very important test cases because they become self-similar far enough downstream from the source and so detailed experimental data of both

mean-flow and turbulence quantities are available for comparison with the numerical predictions. Consequently they will be considered separately hereafter.

The Reynolds number Re at the source in the case of inertia-dominated jets

$$Re = \frac{W_0 D_0}{\nu} \tag{19}$$

and the Grashof number G at the source in the case of buoyancy-dominated jets

$$G = \frac{\beta g D_0^3 (\Theta_0 - \Theta_{N_0})}{\nu^2} \tag{20}$$

are high enough to ensure that the viscous effects are negligible compared to inertia and/or buoyancy effects.

The relative importance of inertial and buoyancy forces at the source can be characterized by the discharge densimetric Froude number F

$$F = \frac{W_0^2}{\beta g D_0 (\Theta_0 - \Theta_{N_0})}. \tag{21}$$

So, in the case of a pure jet $F \approx \infty$ while in the case of a pure plume $F \approx 0$.

4.1. *Turbulent pure jet*

In this section a heated turbulent plane jet exhausting into uniform stagnant surroundings is considered. The temperature may be considered as a passive contaminant and the buoyancy effects are negligible ($F = 10^3$). The Reynolds number at the source is $Re = 3.3 \times 10^7$. A definition sketch of the flow is given in Fig. 3.

Far enough downstream from the source the flow becomes self-similar in the sense that the mean-flow and turbulence profiles become independent of downstream distance when expressed in terms of local characteristic scales:

(a) the velocity half-width $\delta(z)$;
(b) the centre-line velocity $W_m(z)$;
(c) the temperature half-width $\delta_\theta(z)$;
(d) the maximum temperature excess $\Delta\Theta_m(z)$;

which are defined in Fig. 3.

A similarity analysis providing some information on the expected flow behaviour may be carried out (see e.g. ref. [17]) yielding the following relations:

$$\frac{d\delta}{dz} = S_{W_j} \tag{22}$$

$$\frac{d\delta_\theta}{dz} = S_{\theta_j} \tag{23}$$

$$\frac{W_m}{W_0} = A_W \left(\frac{z - z_0}{D_0}\right)^{-1/2} \tag{24}$$

$$\frac{\Delta\Theta_m}{\Delta\Theta_0} = A_\theta \left(\frac{z - z_0}{D_0}\right)^{-1/2} \tag{25}$$

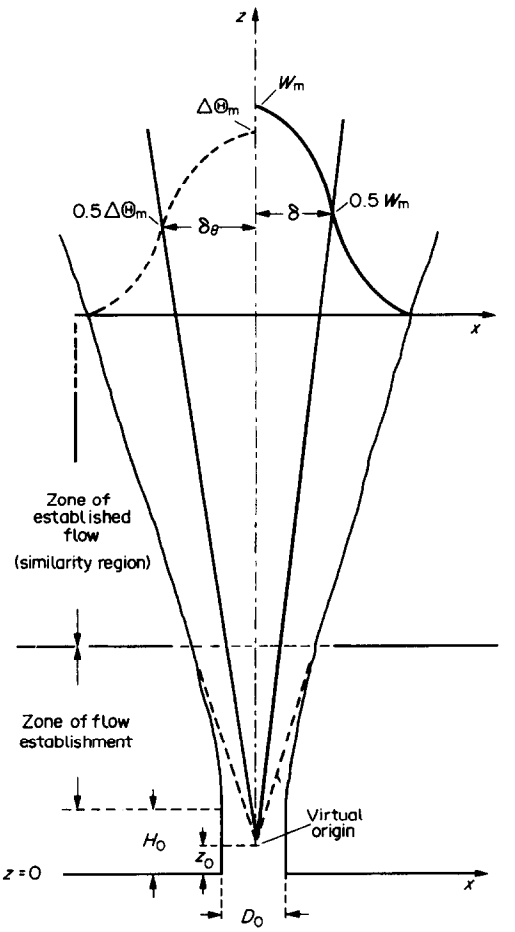

FIG. 3. Definition sketch of the pure jet.

$$\frac{k_{\mathcal{C}}}{W_m^2} = A_k \tag{26}$$

$$\frac{\varepsilon_{\mathcal{C}} \delta}{W_m^3} = A_\varepsilon \tag{27}$$

where S_{W_j}, S_{θ_j}, A_W, A_θ, A_k and A_ε are constants.

Rodi [18], Chen and Rodi [17] and List [19] reviewed mean-flow and turbulence measurements concerning self-similar turbulent jets. For most quantities the experimental data selected for comparison with the computed results are those recommended by these reviewers. The numerical results are also compared with those obtained by Sini [6] using a second-moment turbulence closure model (called below GSHIFT) and with those obtained by Malin and Spalding [20] using a buoyancy-extended version of a k–$\mathcal{W}$ model, $\mathcal{W}$ being the time-mean square of the vorticity fluctuations.

The decay of the centre-line velocity W_m and the maximum temperature excess $\Delta\Theta_m$ are presented in Fig. 4. A relatively close agreement can be observed between experimental and computed results except for a small discrepancy for the centre-line velocity decay in the initial region of the flow which may be due to uncertainties on the levels of turbulence

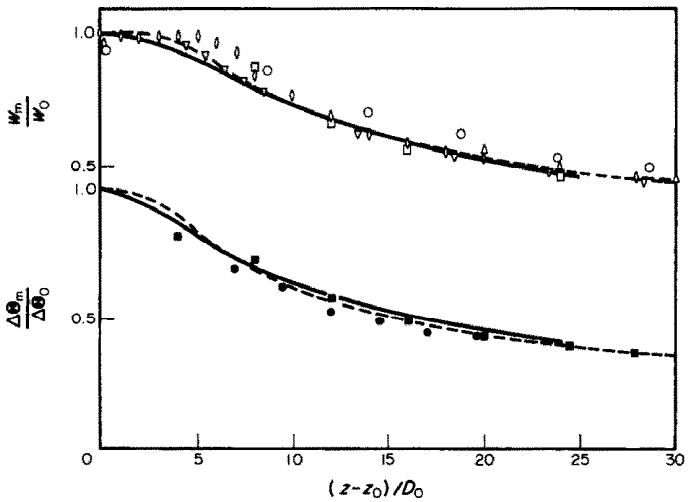

FIG. 4. Decay of centre-line velocity and temperature excess in the pure jet. Experimental data: ○, Bradbury [21]; ●, Davies *et al.* [27]; △, Gutmark and Wygnanski [28]; ▽, Miller and Comings [29]; □, ■, Bashir and Uberoi [30]; ◇, van der Hegge Zijnen [31]. Predictions: ——, JEPHTE (present work); – – –, GSHIFT [6].

Table 2. Longitudinal variations of the main characteristics in self-similar plane jets

	S_{W_j}	S_{θ_j}	A_W	A_θ	A_k	A_ε
Experimental data	0.11 [17]	0.14 [17]	2.4 [17]	2.0 [17]	0.067 [21]	0.014 [21]
JEPHTE present k–ε model	0.10	0.133	2.35	2.02	0.067	0.013
GSHIFT [6] second-moment closure model	0.105	0.108	2.38	1.97	0.06	0.012
k–$\mathscr{W}$ model Malin and Spalding [20]	0.11	0.16	2.51	1.96	0.065	0.0135
k–ε model Hossain and Rodi [22]	0.116	0.154	2.37	2.10	0.068	0.0135

intensities at the exit slot [6]. Downstream ($(z-z_0)/D_0 \geqslant 10$) the results are closely related confirming the validity of the self-similar relations (24) and (25). The decay-law constants A_W and A_θ agree well (Table 2) with the values recommended by Chen and Rodi [17].

The calculated and measured values of the rates of spread of the dynamical and thermal fields, S_{W_j} and S_{θ_j} are also shown in Table 2. Concerning S_{W_j}, the present k–ε model induces the value 0.10, which appears to be a weakly underestimated value when compared with the recommended [18] average experimental value, namely 0.11. But it should be noted that there is a large discrepancy between the experimental data going from 0.087 [23] up to 0.115 [24].

The longitudinal distribution of the turbulent kinetic energy and its dissipation rate at the flow axis are presented dimensionlessly on Fig. 5 together with those obtained by Sini [6] using a second-moment turbulence closure (code GSHIFT). As it can be observed the self-similarity is not completely established for these turbulent quantities at the section $(z-z_0)/D_0 = 25$. Further downstream, the axial dimensionless levels of k and ε tend to stabilize at a constant value according to the similarity laws [26, 27]. As it can be seen (Table 2) none of the various computed values of A_k and A_ε are significantly different from the recommended experimental data.

The following presented results concern the cross-stream similarity profiles of both mean-flow and turbulence quantities. Local characteristic scales are used to normalize all these results which are expressed as dimensionless functions of the dimensionless geometrical variables: $\eta = (x-x_s)/\delta$ for the dynamical field and $\eta_\theta = (x-x_s)/\delta_\theta$ for the thermal field.

Figures 6(a) and (b) show the self-similar profiles of mean velocity and mean temperature excess, respectively. The dashed curves depict computed results obtained with GSHIFT while the symbols represent experimental data. The calculated profiles are in excellent agreement with the experimental data except at the edges of the jet where the temperature excess is clearly overpredicted by the present k–ε model. This has been previously noted by various workers [6, 20, 22]. The observed discrepancy is emphasized when using an unsteady elliptic model because the temperature increases weakly at the edges of the jet due to the transient recirculating motion.

The turbulent kinetic energy self-similar profile is shown in Fig. 7(a). The model predicts the correct level on the centre-line of the jet and also a value of the peak very close to the experimental one. However,

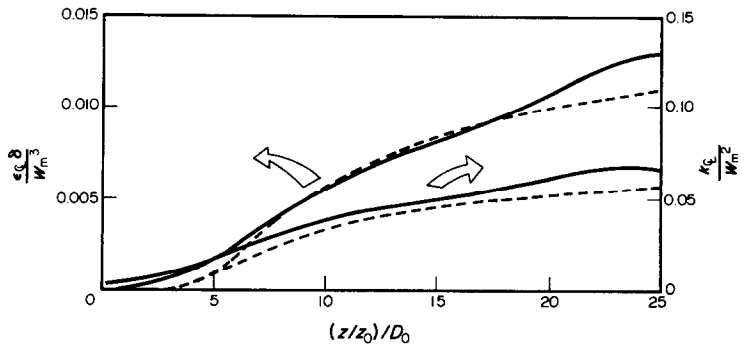

FIG. 5. Longitudinal distribution of the turbulent kinetic energy and its dissipation rate at the pure jet axis. Predictions: ——, JEPHTE (present work); – – – –, GSHIFT [6].

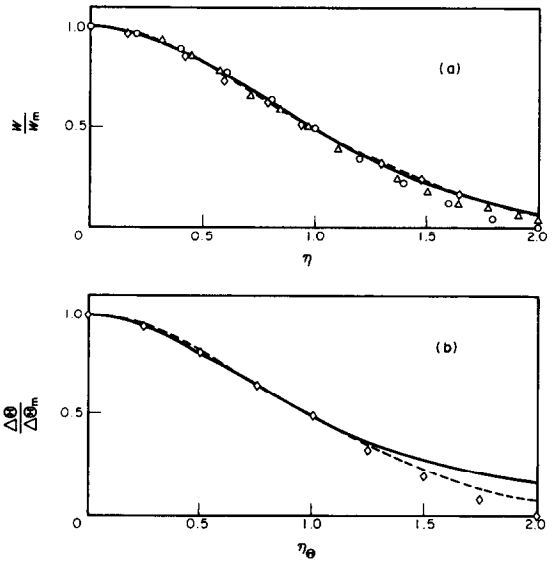

FIG. 6. Similarity profiles in the pure jet: (a) mean velocity, (b) mean temperature excess. Experimental data: ○, Bradbury [21]; ◇, Davies *et al.* [27]; △, Gutmark and Wygnanski [28]. Predictions: ——, JEPHTE (present work); – – – –, GSHIFT [6].

a very notable discrepancy appears near the edge of the flow. This is clearly connected with the level of turbulence intensity initially present in the ambient fluid. Presently the uniform ambient turbulence intensity was set as $k/W_0^2 = 2.8 \times 10^{-3}$, which may be written according to equation (24) as

$$\frac{k}{W_0^2} = 5 \times 10^{-4}\left(\frac{z-z_0}{D_0}\right).$$

Therefore, in the section concerned in Fig. 7(a) the turbulence intensity at the edge of the flow must be about 1.25×10^{-2}, making clear the discordance in question.

It is of interest to consider the turbulent energy balance. The predicted distributions shown in Fig. 7(b) display a very satisfactory agreement with the measurements of Bradbury [21].

Figure 8 shows that the similarity profile of the dissipation rate ε predicted by JEPHTE is not significantly different from those obtained by Malin and Spalding [20] and Hossain and Rodi [22]. The experimental profile of Bradbury [21] has a smoother shape than the computed one but the comparison is satisfactory.

4.2. *Turbulent pure plume*

In this section, the flows considered are vertical plane plumes with a density lower than that of the uniform stagnant environment.

In a fully turbulent plume ($G \gg 1$) the character of the flow is determined by the discharge densimetric Froude number F. Attention is here restricted to the limiting case of the pure plume ($F \approx 0$) where the initial momentum is either zero or negligible.

Like the pure jet, the pure plume has a tendency to become self-similar after a certain development region. The similarity analysis yields the following laws [17]:

$$\frac{d\delta}{dz} = S_{W_p} \tag{28}$$

$$\frac{d\delta_\theta}{dz} = S_{\theta_p} \tag{29}$$

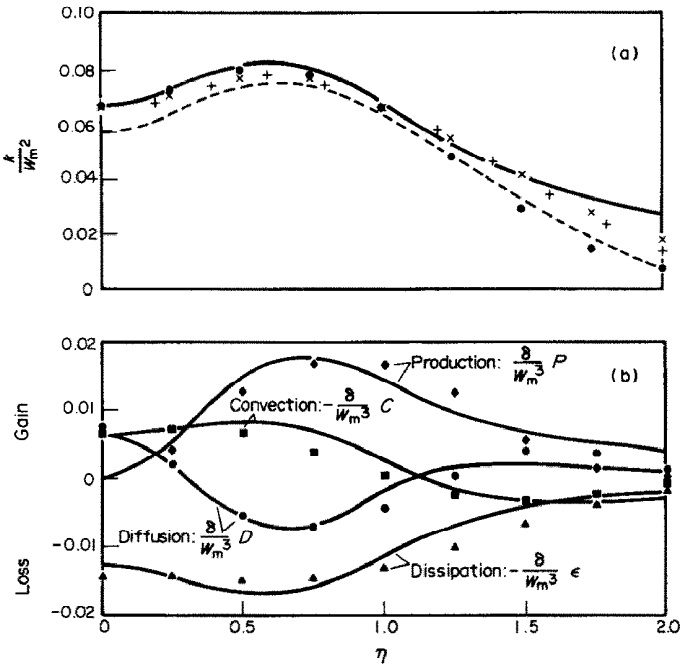

FIG. 7. Similarity profile of turbulent kinetic energy (a) and turbulent kinetic energy balance (b) in the pure jet. Experimental data: Bradbury [21]: dark symbols. Predictions: +, Malin and Spalding [20]; ×, Hossain and Rodi [22]; ——, JEPHTE (present work); – – – –, GSHIFT [6].

$$\frac{W_m}{W_0} = B_W F^{-1/3}\left(\frac{\rho_0}{\rho_N}\right)^{1/3} \tag{30}$$

$$\frac{\Delta\Theta_m}{\Delta\Theta_0} = B_\theta F^{1/3}\left(\frac{\rho_0}{\rho_N}\right)^{-1/3}\left(\frac{z-z_0}{D_0}\right)^{-1} \tag{31}$$

$$\frac{k_\mathbb{C}}{W_m^2} = B_k \tag{32}$$

$$\frac{\varepsilon_\mathbb{C}\delta}{W_m^3} = B_\varepsilon. \tag{33}$$

Numerical results concerning the decay-laws, equations (30) and (31), have been previously reported by Hossain and Rodi [22] and by Chen and Chen [25] using buoyancy extended versions of the k–ε or k–ε–$\overline{\theta^2}$ turbulence models through algebraic stress/flux modelling (ASM), and by Malin and Spalding [20] using a k–$\mathscr{W}$–$\overline{\theta^2}$ model.

Table 3 shows the comparisons concerning the decay law constants B_W and B_θ. As can be observed the numerical predictions obtained with the standard k–ε model JEPHTE ($C_\mu = 0.09$) are consistently higher than the recommended experimental data [17]. More satisfactory results are obtained when C_μ is sensitive to the buoyancy discharge via functional relationship (15). Furthermore, for the flow considered, the comparison with models using ASM relations is then not unfavorable to JEPHTE.

The ability of the present model with $C_\mu = f(F)$ to produce the correct relative behaviour as regards velocity and temperature is improved as can be seen in Table 4. The spreading rates S_{W_p} and S_{θ_p} work in

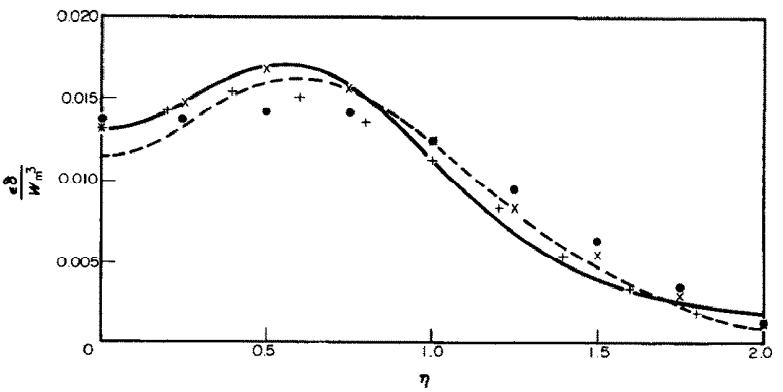

FIG. 8. Similarity profile of the dissipation rate ε in the pure jet. For legend, see Fig. 7.

Table 3. Decay-law constants in a pure plume

	B_w	B_θ
Recommended experimental data [17]	1.9	2.4
JEPHTE $C_\mu = 0.09$	2.31	2.66
JEPHTE $C_\mu = f(F)$ (15)	2.10	2.43
k–ε with ASM (Hossain and Rodi [22])	1.98	2.60
k–ε–θ^2 with ASM (Chen and Chen [25])	2.28	2.15
k–$\mathscr{W}$–θ^2 (Malin and Spalding [20])	2.03	2.43

Table 4. Spreading rates in a pure plume

	S_{wp}	$S_{\theta p}$
Recommended experimental data [17]	0.12	0.13
JEPHTE $C_\mu = f(F)$ (15)	0.112	0.129
k–ε with ASM (Hossain and Rodi [22])	0.127	0.125
k–$\mathscr{W}$–θ^2 (Malin and Spalding [20])	0.121	0.135

fairly good agreement with experimental values. Nevertheless the predicted level of the centre-line velocity remains somewhat too high when compared to experimental data.

The predicted mean velocity and mean temperature excess are compared in Fig. 9 with the experimental data of Rouse *et al.* [26]. As already observed in the case of a pure jet (Fig. 6(b)) the temperature is patently overestimated at the edge of the flow. The same numerical reasons mentioned in Section 4.1 can be cited here.

Figure 10(a) shows the predicted similarity profile of the turbulent kinetic energy k. Unfortunately in pure plume situations experimental measurements are not available so that a direct comparison is not possible. For comparative purposes, numerical results obtained by Hossain and Rodi [22] and Malin and Spalding [20] are also plotted. A very large discrepancy appears near the centre of the plume, JEPHTE predicts values about 45% lower than those obtained with other models. The dimensionless centre-line levels of k are specified in Table 5 together with those of ε.

The computed turbulent kinetic energy balance shown in Fig. 10(b) is to compare with the one (Fig. 7(b)) achieved in the pure jet case. At the plume axis, not only the production term goes to zero but also the convection term since the centre-line velocity is invariant with height. Therefore, the dissipation is only balanced by the diffusion. As can be seen the buoyancy production term B, equation (13), is not significant everywhere across the flow. That is at variance with the predictions of Hossain and Rodi [22] and Malin and Spalding [20] who both obtained $B/\mathscr{P} \approx 1/3$. This discrepancy probably explains the self-similar profile of k (Fig. 10(a)).

The buoyancy-production term, equation (13), involves the vertical turbulent heat flux $\overline{w\theta}$ originating in the buoyancy term of the Navier–Stokes equations from which the k-equation is derived. The present model makes use of an eddy diffusivity concept, equation (6), which takes into account buoyancy effects in the k-equation only through the vertical gradient of the mean temperature. This gradient is important during the transient period when the plume starts but falls to a very weak level on the axis of the steady established flow. Moreover, $\partial\Theta/\partial z$ changes sign across the plume producing a slight negative contribution of the buoyancy term in the outer area of the flow, i.e. $\eta > 0.5$ in Fig. 10(b). Although there is no reference data about heat flux in a pure plume it appears implausible that $\overline{w\theta}$ becomes negative under the buoyancy influence.

In spite of this restriction, the present work shows that the proposed model is suitable to correctly predict the mean behaviour of a vertical plane pure plume.

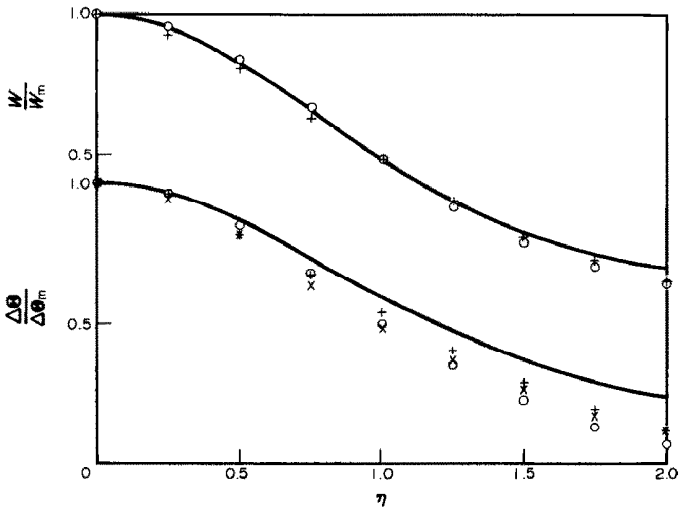

FIG. 9. Similarity profiles of mean velocity and mean temperature excess in the pure plume. Experimental data: ○, Rouse *et al.* [26]. Predictions: +, Malin and Spalding [20]; ×, Hossain and Rodi [22]; ——, JEPHTE (present work).

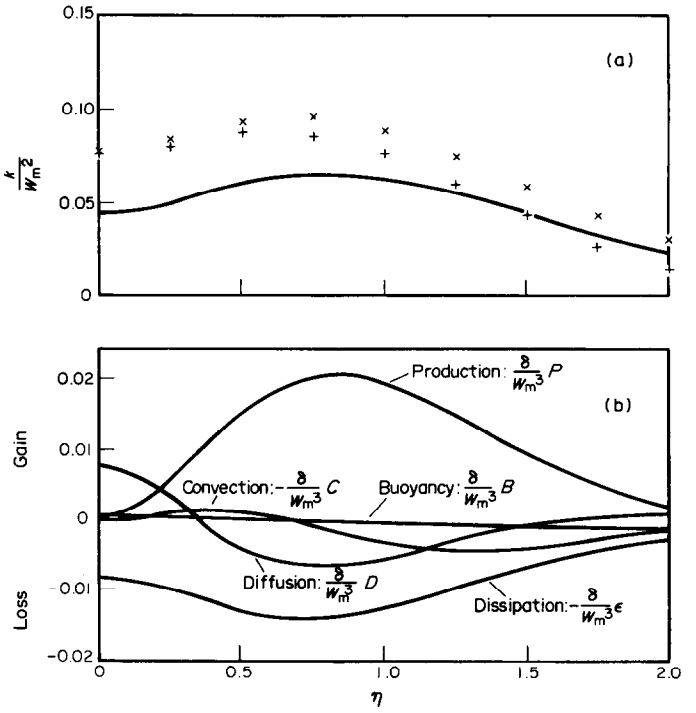

FIG. 10. Similarity profile of turbulent kinetic energy (a) and turbulent kinetic energy balance in the pure plume (b). For legend see Fig. 9.

Table 5. Computed centre-line levels of k and ε in a pure plume

	$B_k = \frac{k_c}{W_m^2}$	$B_\varepsilon = \frac{\varepsilon_c \delta}{W_m^3}$
JEPHTE (present work)	4.4×10^{-2}	0.86×10^{-2}
k–ε with ASM (Hossain and Rodi [22])	7.7×10^{-2}	1.43×10^{-2}
k–ε–θ^2 with ASM (Chen and Chen [25])	8.5×10^{-2}	1.2×10^{-2}
k–ω–θ^2 (Malin and Spalding [20])	7.5×10^{-2}	1.46×10^{-2}

4.3. *Turbulent forced plumes*

In this section the general situation of the buoyant jet is considered where there are present both initial momentum and buoyancy. The character of the flow is determined by the densimetric Froude number F at the exit. In a uniform stagnant environment, a forced plume behaves like a non-buoyant jet near the source (jet region) but like a pure plume in the far field (plume region) even if F is large. The jet and plume regions are separated by a transition region in which self-similarity cannot exist.

Chen and Rodi [17] have proposed a universal scaling law for all three regions of plane forced plumes. They have introduced the following scaling quantities:

$$\begin{cases} z_r = D_0 F^{2/3} (\rho_0/\rho_N)^{1/3} \\ W_r = W_0 F^{-1/3} (\rho_0/\rho_N)^{1/3} \\ \Delta\Theta_r = \Delta\Theta_0 F^{-1/3} (\rho_0/\rho_N)^{-2/3} \end{cases} \quad (34)$$

to normalize various experimental data and present them in a unified way so as to allow an easy comparison between predictions and measurements. In the present section, the same scaling quantities are used to normalize the calculated decay of the mean velocity and the mean temperature excess along the axis of the jet.

The calculations are performed for densimetric Froude numbers F of 1000, 250, 100, 25, 10, 5, 2, 1 and 0.5 so as to cover the full range between pure jet and pure plume. In each case, the inlet conditions are chosen in order to define the appropriate Froude number.

Figure 11 compares the predicted results (symbols) with the experimental data (full lines) recommended by Chen and Rodi [17] in their very useful review of measurements concerning vertical turbulent buoyant jets. Their recommendations are

jet region: $z - z_0 < 0.5 z_r$

$$\frac{W_m}{W_r} = A_W \left(\frac{z - z_0}{z_r} \right)^{-1/2} \quad \text{with} \quad A_W = 2.4 \quad (35)$$

$$\frac{\Delta\Theta_m}{\Delta\Theta_r} = A_\theta \left(\frac{z - z_0}{z_r} \right)^{-1/2} \quad \text{with} \quad A_\theta = 2.0; \quad (36)$$

plume region: $z - z_0 > 5.0 z_r$

$$\frac{W_m}{W_r} = B_W \quad \text{with} \quad B_W = 1.9 \quad (37)$$

$$\frac{\Delta\Theta_m}{\Delta\Theta_r} = B_\theta \left(\frac{z - z_0}{z_r} \right)^{-1} \quad \text{with} \quad B_\theta = 2.4. \quad (38)$$

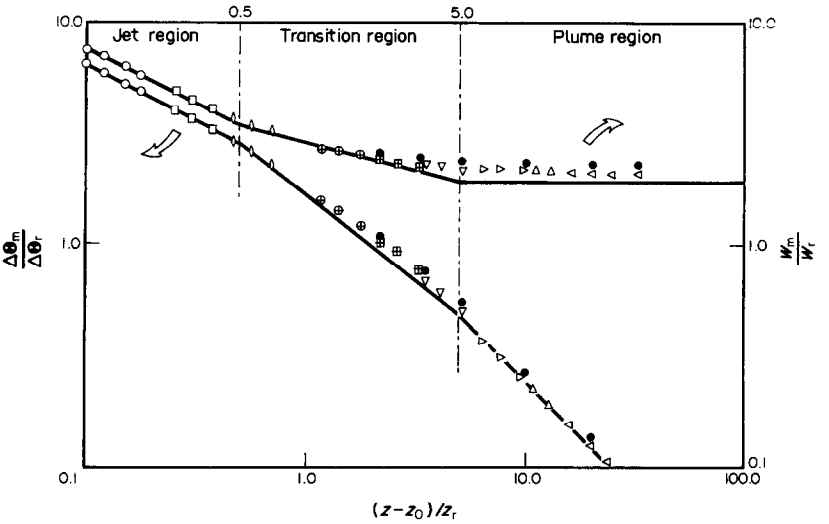

FIG. 11. Decay of centre-line velocity and temperature excess in plane forced plumes. ——, Recommended experimental data [17]. Predictions: ●, $C_\mu = 0.09$; $C_\mu = f(F)$: ◁, $F = 0.5$; △, $F = 1$; ▷, $F = 2$; ▽, $F = 5$; ⊞, $F = 10$; ⊕, $F = 25$; ◇, $F = 100$; □, $F = 250$; ○, $F = 1000$.

Since only established flow is concerned with similarity laws, numerical results are plotted in Fig. 11 only for $z - z_0 \geqslant 10D_0$. A gradual change from jet-like to plume-like behaviour is observed which is in close agreement with the experimental data. However, as already shown in Table 3, calculations with lower Froude numbers overpredict the centre-line velocity ($W_m/W_r = 2.10$) with respect to the experimental level ($W_m/W_r = 1.90$). In Fig. 11, the dark symbols depict computed results obtained with the standard model ($C_\mu = 0.09$). From Fig. 11 it can be seen that the predicted limits of the transition region agree with the recommended ones by Chen and Rodi [17].

The scaling quantities (34) may be used to normalize the centre-line values of the turbulent kinetic energy k and its dissipation rate ε; the similarity laws yielding the following relations:

jet region: $z - z_0 < 0.5 z_r$

$$\frac{k_{\mathrm{CL}}}{W_r^2} = A_k A_W^2 \left(\frac{z-z_0}{z_r}\right)^{-1} \tag{39}$$

$$\frac{\varepsilon_{\mathrm{CL}} z_r}{W_r^3} = \frac{A_\varepsilon A_W^3}{S_{W_j}} \left(\frac{z-z_0}{z_r}\right)^{-5/2}; \tag{40}$$

plume region: $z - z_0 > 5.0 z_r$

$$\frac{k_{\mathrm{CL}}}{W_r^2} = B_k B_W^2 \tag{41}$$

$$\frac{\varepsilon_{\mathrm{CL}} z_r}{W_r^3} = \frac{B_\varepsilon B_W^3}{S_{W_p}} \left(\frac{z-z_0}{z_r}\right)^{-1}. \tag{42}$$

Figures 12 and 13 show the variations of these centre-line dimensionless variables with height. It can be seen in both figures that, except in the zone of flow establishment, all predictions fall into a single curve when the flow becomes established. In the jet region and in the plume region, the predictions verify the respective similarity decay laws, equations (39)–(42).

5. CONCLUDING REMARKS

A buoyancy-extended k–ε model of turbulence has been developed in the present work for calculating turbulent plane jets and plumes issuing in a uniform stagnant environment. The model solves transport equations for the turbulent kinetic energy k and its dissipation rate ε, completing the set of equations governing the velocity and temperature distribution. The mathematical model forms a closed unsteady system of elliptic partial differential equations solved by an MAC method [12].

The buoyancy-extended version of the k–ε turbulence model provides satisfactory predictions of the flow in self-similar jets.

In the limiting case of the pure plume, an empirical relation assuming C_μ to be influenced by buoyancy was introduced. This improves significantly the model's ability to describe the mean flow characteristics. However, in a steady established plume the predicted turbulent energy budget reveals a slight negative contribution from the buoyant production term. Although no experimental data is available concerning the turbulent kinetic energy in a pure plume, this result—originating from the adopted eddy diffusivity assumption—appears implausible. Grappling with more complex buoyant flows, it would probably be suitable to develop a refined modelling of buoyancy effects as those discussed by Rodi [1].

Nevertheless the present model was seen to predict the mean dynamical and thermal fields in vertical plane buoyant jets with an accuracy sufficient for practical purposes.

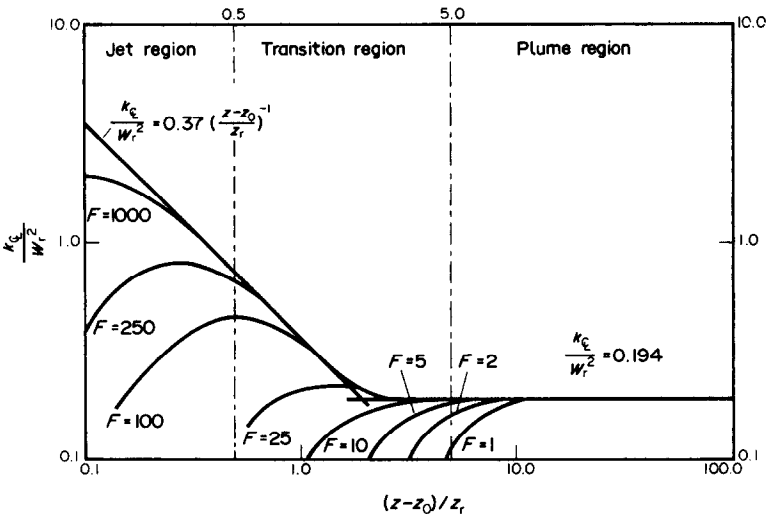

FIG. 12. Decay of centre-line turbulent kinetic energy in plane forced plumes: ——, predictions JEPHTE (present work).

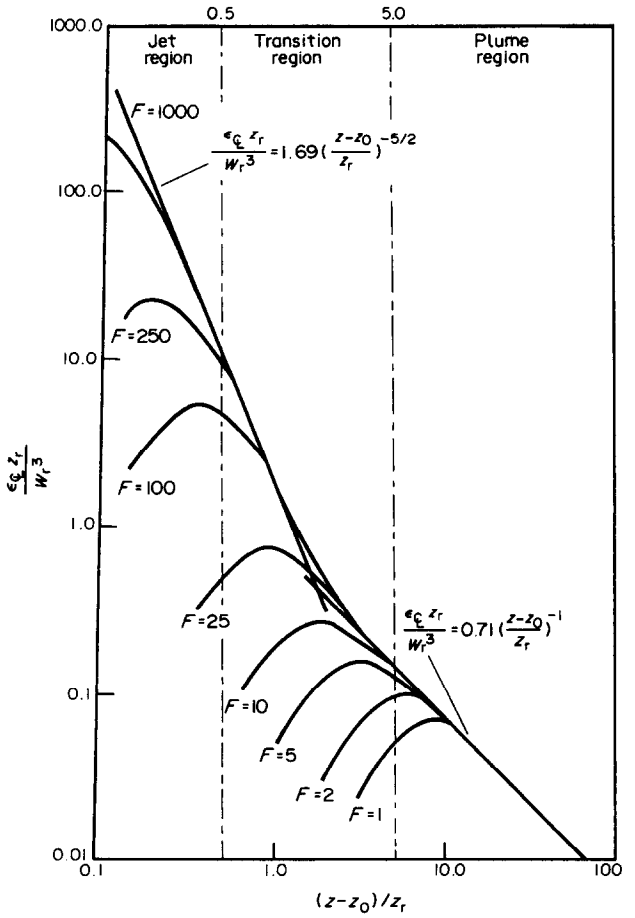

FIG. 13. Decay of centre-line dissipation rate in plane forced plumes: ——, predictions JEPHTE (present work).

Further work on the application of this model to 2-D and 3-D turbulent buoyant jets vertically or horizontally discharging into a stably stratified ambient fluid is actually in progress.

The primary results [6] concerning a 2-D forced plume issuing vertically into a linearly stratified stagnant or horizontally flowing environment are very encouraging. So the model will be applied in the future

to further more practical studies about the discharge of sewage effluent from a line source into a stratified ocean.

Acknowledgements—The present work made use of a modified version of the program GEDEON developed at Electricité de France. The authors wish to express their grateful thanks to M. P. Mery, Head of Division Météorologie Appliquée et Pollution Atmosphérique, Electricité de France, for providing us with a basic 3-D version of the computer code. We acknowledge helpful discussions with P. Biscay supporting documentation about the original program. The numerical calculations were carried out on the CRAY IS/1000 at Ecole Polytechnique, 91128 Palaiseau, France. Complete computer support was given by the Scientific Council of Centre de Calcul Vectoriel pour le Recherche.

REFERENCES

1. W. Rodi, *Turbulence Models and their Application in Hydraulics: a State of the Art Review*. Book Publication of International Association for Hydraulic Research, Delft, The Netherlands (1980).
2. M. M. Gibson and B. E. Launder, On the calculation of horizontal turbulent shear flows under gravitational influence, *Trans. Am. Soc. Mech. Engrs*, Series C, *J. Heat Transfer* 81–87 (1976).
3. J. C. Chen and W. Rodi, A mathematical model for stratified turbulent flows and its application to buoyant jets, *Proc. 16th Congress IAHR*, Sao Paulo, Brasil (1975).
4. G. Batchelor, *An Introduction to Fluid Dynamics*. Cambridge University Press, Cambridge (1970).
5. J. J. McGuirk and W. Rodi, The calculation of 3-D turbulent free jets. In *Turbulent Shear Flow*, Vol. 1. Springer, Heidelberg (1979).
6. J. F. Sini, Modélisation d'écoulements turbulents libres bidimensionnels avec effets de flottabilité—cas du panache en milieu stratifié, Thèse de Doctorat de l'Université d'Aix-Marseille II (1986).
7. J. F. Sini and I. Dekeyser, Prévision numérique de jets 2-D en milieux stratifiés à l'aide d'un modèle k–ε, Note I.M.S.T. 2/86 (1986).
8. R. Schiestel, Modélisation des écoulements turbulents, Cours I.M.S.T., Université d'Aix-Marseille II (1982).
9. K. Hanjalic and B. E. Launder, A Reynolds stress model of turbulence and its application to thin shear flows, *J. Fluid Mech.* **52,** 609–638 (1972).
10. B. E. Launder and D. B. Spalding, *Lectures in Mathematical Models of Turbulence*, Academic Press, New York (1972).
11. B. E. Launder and D. B. Spalding, The numerical computation of turbulent flow, *Comp. Meth. Appl. Mech. Engng* **3,** 269 (1974).
12. F. H. Harlow and J. E. Welsh, Numerical calculation of time-dependent viscous incompressible flow of fluid with free surface, *Physics Fluids* **8,** 2182–2189 (1965).
13. C. W. Hirt and F. H. Harlow, A general corrective procedure for the numerical solution of initial value problems, *J. Comput. Phys.* **2,** 114–119 (1967).
14. A. J. Chorin, A numerical method for solving incompressible viscous flow problems, *J. Comput. Phys.* **2,** 12–26 (1967).
15. R. Peyret and T. D. Taylor, *Computational Methods for Fluid Flow*. Springer, New York (1983).
16. P. Gaillard, Modélisation numérique des panaches d'aéroréfrigérant, Thèse de Docteur Ingénieur, Laboratoire de Mécanique des Fluides, Ecole Centrale de Lyon (1978).
17. C. J. Chen and W. Rodi, *Vertical Turbulent Buoyant Jets, a Review of Experimental Data*. Pergamon Press, London (1980).
18. W. Rodi, A review of experimental data of uniform density free turbulent boundary layers. In *Studies in Convection* (Edited by B. E. Launder), Vol. 1. Academic Press, New York (1975).
19. E. J. List, Mechanics of turbulent buoyant jets and plumes. In *Turbulent Buoyant Jets and Plumes*, Vol. 6. Pergamon Press, Oxford (1982).
20. M. R. Malin and D. B. Spalding, The prediction of turbulent jets and plumes by use of the $k-\overline{w'}$ model of turbulence, *Physico-chem. Hydrodyn.* **5,** 153–198 (1984).
21. L. J. S. Bradbury, The structure of a self-preservating turbulent plane jet, *J. Fluid Mech.* **23,** 31–61 (1965).
22. M. S. Hossain and W. Rodi, A turbulence model for buoyant flows and its application to vertical buoyant jets. In *Turbulent Buoyant Jets and Plumes*, Vol. 6. Pergamon Press, Oxford (1982).
23. N. E. Kotsovinos, A study of the entrainment and turbulence in a plane buoyant jet, Ph.D. thesis, California Institute of Technology, Pasadena, California (1975).
24. J. Bicknell, A study of turbulent mixing between a plane jet of fluid of various densities and still fluid, M.Sc. thesis, Massachusetts Institute of Technology, Cambridge, Massachusetts (1937).
25. C. J. Chen and C. H. Chen, On predictions and unified correlation for decay of vertical buoyant jets, *J. Heat Transfer* **101,** 532–537 (1979).
26. H. Rouse, C. S. Yih and H. W. Humphreys, Gravitational convection from a boundary source, *Tellus* **4,** 201–210 (1952).
27. A. E. Davies, J. F. Keffer and W. D. Baines, Spread of a heated plane turbulent jet, *Physics Fluids* **18,** 770–775 (1975).
28. E. Gutmark and I. Wygnanski, The planar turbulent jet, *J. Fluid Mech.* **73,** 465–495 (1976).
29. D. R. Miller and E. W. Comings, Static pressure distribution in the free turbulent jet, *J. Fluid Mech.* **3,** 1–16 (1957).
30. J. Bashir and M. S. Uberoi, Experiments on turbulent structure and heat transfer in a two-dimensional jet, *Physics Fluids* **18,** 405–410 (1975).
31. B. G. van der Hegge Zijnen, Measurements of the distribution of heat and matter in a plane turbulent jet of air, *Appl. Scient. Res.* **A7,** 277–292 (1958).

PREVISION NUMERIQUE DE JETS 2-D, PORTANTS OU NON, A L'AIDE D'UN MODELE DE TURBULENCE DE TYPE k–ε

Résumé—Un modèle de type k–ε incluant les effets de flottabilité a été développé afin de réaliser la prévision numérique des champs dynamique et thermique de jets 2-D, portants ou non, s'épanouissant dans un milieu uniforme au repos. Le système résultant, d'équations aux dérivées partielles (continuité, quantité de mouvement, température, k énergie cinétique de la turbulence et ε son taux de dissipation), instationnaire et à caractère elliptique dans l'espace est traité au moyen d'un code approprié dénommé JEPHTE. Une version prenant en compte une influence de la portance du jet sur la viscosité équivalente ν_T due à la turbulence a été testée; une relation empirique pour le coefficient C_μ en fonction du nombre de Froude à la source a été introduite. Les résultats numériques du modèle sont comparés aux résultats expérimentaux et à ceux obtenus avec des modélisations plus élaborées pour la prise en compte des effets de flottabilité.

NUMERISCHE BERECHNUNG TURBULENTER EBENER STRAHLEN UND ERZWUNGENER STRÖMUNGSFAHNEN MIT HILFE DES k–ε-TURBULENZMODELLS

Zusammenfassung—Es wurde ein um den Auftrieb erweitertes k–ε-Turbulenzmodell entwickelt, mit dem das Temperatur- and Geschwindigkeitsfeld in ebenen turbulenten Strahlen und erzwungenen Strömungsfahnen bei einheitlichem ruhendem Umgebungszustand berechnet werden kann. Die den Prozeß beschreibenden partiellen Differentialgleichungen (Kontinuität, Quer- und Längsimpuls, thermische Energie, kinetische Turbulenzenergie k und zugehörige Dissipationsrate ε) werden mit Hilfe eines Computerprogramms für elliptische unstetige Differentialgleichungen gelöst. Es wurde eine Version untersucht, bei der C_μ als empirische Funktion der densimetrischen Froude-Zahl der Quelle angenommen wird. Die Berechnungen werden verglichen mit experimentellen Daten und/oder Ergebnissen, die mit komplexeren Modellen des Auftriebseffekts ermittelt wurden.

РАСЧЕТ ТУРБУЛЕНТНЫХ ПЛОСКИХ ВЫНУЖДЕННЫХ И СВОБОДНО-КОНВЕКТИВНЫХ СТРУЙ С ПОМОЩЬЮ k–ε МОДЕЛИ ТУРБУЛЕНТНОСТИ

Аннотация—Использована k–ε модель турбулентности с учетом силы плавучести для расчета полей скорости и температуры в плоских турбулентных вынужденных и свободно-конвективных струях в однородной неподвижной среде. С помощью эффективной численной схемы для эллиптических нестационарных дифференциальных уравнений решены определяющие дифференциальные уравнения в частных производных (неразрывности, сохранения количества движения, тепловой «энергии», турбулентной кинетической энергии k и скорости ее диссипации ε). Проверено предположение, согласно которому C_μ есть эмпирическая функция числа Фруда для источника. Проведено сравнение результатов расчетов с экспериментальными данными и численными результатами, полученными для более сложных моделей.